MOLECULAR IMAGING AND BIOLOGY

Mol Imaging Biol (2019) 21:740–746
DOI: 10.1007/s11307-018-1283-y

Published Online: 3 October 2018

RESEARCH ARTICLE

Histogram Analysis Parameters Derived from Conventional T1- and T2-Weighted Images Can Predict Different Histopathological Features Including Expression of Ki67, EGFR, VEGF, HIF-1α, and p53 and Cell Count in Head and Neck Squamous Cell Carcinoma

Hans Jonas Meyer,[1] Leonard Leifels,[1] Gordian Hamerla,[1] Anne Kathrin Höhn,[2] Alexey Surov[1]

[1]*Department of Diagnostic and Interventional Radiology, University of Leipzig, Liebigstraße 20, 04103, Leipzig, Germany*
[2]*Department of Pathology, University of Leipzig, Liebigstraße 26, 04103, Leipzig, Germany*

Abstract

Purpose: To analyze associations between histogram analysis parameters derived from conventional magnetic resonance imaging (MRI) and different histopathological features in head and neck squamous cell carcinoma (HNSCC).

Procedures: Thirty-four patients with histologically proven primary HNSCC were prospectively acquired. Histogram analysis was derived from pre-contrast T1-weighted (T1w) and T2-weighted (T2w) images. In all cases, expression of HIF-1α, VEGF, EGFR, p53, Ki67, and p16 as well as tumor cell count was analyzed.

Results: In the overall sample, inverse correlation between entropy derived from T1w images and p53 expression ($p = -0.458$, $P = 0.01$) was found. Furthermore, p10 derived from T1w images correlated with VEGF expression ($p = 0.371$, $P = 0.04$). In the p16-positive tumors, VEGF expression correlated with several parameters derived from T1w images: mean ($p = 0.481$, $P = 0.032$), p10 ($p = 0.489$, $P = 0.029$), p25 ($p = 0.475$, $P = 0.034$), median ($p = 0.468$, $P = 0.037$), and mode ($p = 0.492$, $P = 0.028$). Several T2w parameters were associated with p53 expression: mean ($p = 0.569$, $P = 0.007$), p25 ($p = 0.508$, $P = 0.019$), p75 ($p = 0.479$, $P = 0.028$), median ($p = 0.555$, $P = 0.009$), and mode ($p = 0.468$, $P = 0.033$). Kurtosis derived from T2w images correlated with cell count ($p = 0.534$, $P = 0.013$). In p16-negative carcinomas, T2w parameters correlated with p53 expression: max ($p = 0.736$, $P = 0.015$), p90 ($p = 0.687$, $P = 0.028$), and standard deviation ($p = 0.760$, $P = 0.011$). T2w p10 ($p = -0.709$, $P = 0.022$) and T2w p25 ($p = -0.733$, $P = 0.016$) correlated also with HIF-1α expression.

Conclusions: Multiple associations between histogram parameters derived from T1w and T2w images and clinically relevant histopathological features were found in HNSCC. Therefore, imaging parameters can be also used as surrogate markers for tumor cellularity, proliferation, and vascularization in HNSCC. The identified correlations differed significantly between p16-positive and p16-negative cancers.

Key words: Head and neck cancer, MRI, Histogram analysis, p16, Ki67

Correspondence to: Hans Meyer; *e-mail:* Hans-Jonas.Meyer@medizin.uni-leipzig.de

Introduction

Head and neck squamous cell carcinoma (HNSCC) is one of the most frequent malignancies [1]. There is increasing evidence that imaging modalities do not only provide information regarding local tumor localization, metastatic spread, and infiltration of adjacent structure, but also further characterize tumor behavior and microstructure using modern analysis techniques [2]. Thereby, prediction of several histological features in tumors, as well as prediction of treatment and new prognostic biomarkers, is possible and can be implemented into clinical routine [3, 4].

Previously, functional magnetic resonance imaging (MRI) modalities like diffusion-weighted imaging (DWI) or dynamic contrast-enhanced MRI (DCE-MRI) were widely used for prediction of histopathology of several tumors [5–7]. It has been shown that apparent diffusion coefficient (ADC) can reflect cellularity, whereas DCE-MRI parameters can predict microvessel density in tissues [5–7]. Also in HNSCC, these MRI modalities can be used to predict several histopathological features [8–10].

For a short time, an emergent imaging analysis, namely, histogram analysis, has been established. With this approach, every voxel of a ROI is issued into a histogram and, therefore, statistical information can be obtained, and thusly tumors can be better characterized [11]. Presumably, histogram heterogeneity might display heterogeneity of the tumor. This approach was performed predominantly on ADC maps to better predict tumor behavior in several tumor entities [12–14]. However, some authors also used this imaging analysis on conventional MR images [15–18].

According to the literature, different histopathological features are clinically relevant in HNSCC [19–21]. Most important are the following parameters: p16 protein, proliferation index Ki67, epidermal growth factor receptor (EGFR), vascular endothelial growth factor (VEGF), hypoxia-inducible factor (HIF)-1α, and tumor suppressor protein p53 [19–21]. These histopathological features are linked to prognosis and different tumor behaviors in HNSCC [19–21]. Presumably, conventional MR imaging might also be able to reflect those expression profiles.

Therefore, our purpose was to analyze possible associations between histogram parameters derived from conventional MRI sequences and several clinically relevant histopathological features in HNSCC.

Materials and Methods

This prospective study was approved by the institutional review board (ethics committee of the University of Leipzig, study codes 180-2007, 201-10-12072010, and 341-15-05102015). All methods were performed in accordance with the relevant guidelines and regulations. All patients gave their written informed consent.

Patients

Overall, 34 patients with primary HNSCC of different localizations were involved in the study. There were 9 (26 %) women and 25 (74 %) men with a mean age of 56.7 ± 10.2 years, range 33–77 years. At initial presentation, the tumors were localized in the tonsil (23.6 %), followed by those in the oropharynx (20.6 %) and the tongue (20.6 %), the hypopharynx (17.6 %), the larynx (14.6 %), and the nasopharynx (2.9 %). In most cases, high-grade (G3) lesions (51.8 %) were diagnosed. Furthermore, most frequently, the identified lesions were staged as T3 (29.4 %) or T4 (47.1 %) tumors with additional nodal (91.2 %) metastases.

MRI

All imaging were performed using a 3T scanner (Siemens Biograph mMR, Siemens Healthcare, Erlangen, Germany) and a combined head and neck coil. For this study, the following sequences were analyzed: an axial T1-weighted (T1w) turbo spin echo (TSE) sequence (TR 780 ms, TE 12 ms, flip angle 140 °, 42 slices, 4-mm slice thickness, 280-mm field of view, 280 × 233 mm matrix, 1.1 × 0.5 × 4.0 mm voxel size) and an axial T2-weighted (T2w) TSE (TR 5640 ms, TE 105 ms, flip angle 140 °, 42 number of slices, 4-mm slice thickness, 280-mm field of view, 280 × 233 mm matrix, 0.8 × 0.5 × 4.0 voxel size).

Imaging Analysis

For every lesion, T1w and T2w maps were saved in DICOM format and processed offline with custom-made Matlab-based application (The Mathworks, Natick, MA) on a standard Windows system. On the next step, on the saved maps, a volume of interest was drawn at tumor boundary using all slices (whole lesion measure, Fig. 1a–d) as reported previously [12]. All measures were performed by two authors (GH, 2 years of radiological experience, and AS, 15 years of radiological experience) in consensus. For every image, the following parameters were calculated: mean; maximum; minimum; median; mode; and 10th, 25th, 75th, and 90th percentiles as well as kurtosis, skewness, and entropy.

Histopathological Findings

For this study, the biopsy specimens were deparaffinized, rehydrated, and cut into 5-µm slices. On the next step, the histological slices were stained by MIB-1 monoclonal antibody (DakoCytomation, Glostrup, Denmark), epidermal growth factor receptor (EGFR, EMERGO Europe, clone 111.6, dilution 1:30), vascular endothelial growth factor (VEGF, EMERGO Europe, clone VG1, dilution 1:20), tumor suppressor protein p53 (DakoCytomation, Glostrup,

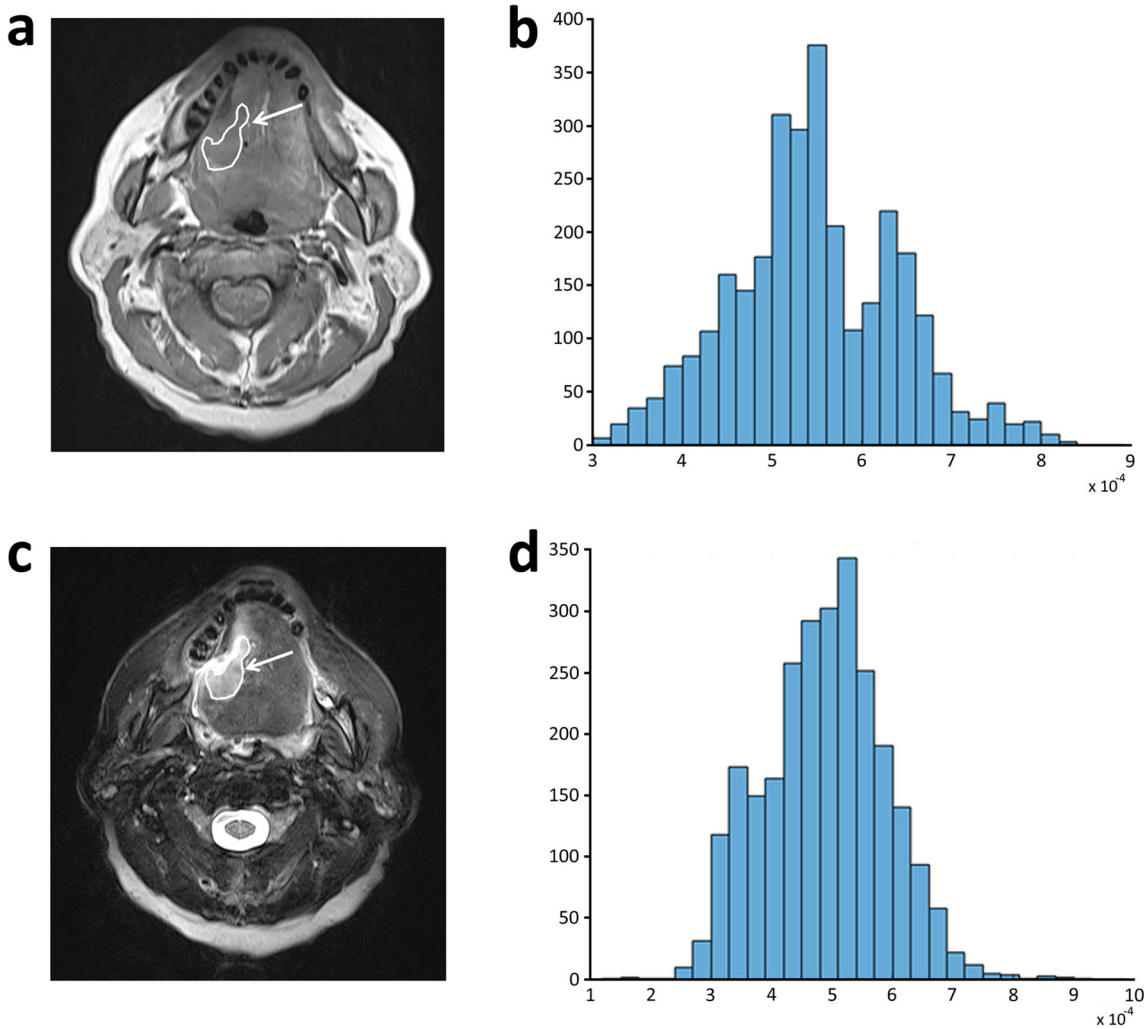

Fig. 1. Radiological findings in a patient with HNSCC of the oral cavity. **a** T1-weighted image without contrast medium application. Axial slide of a case with a cancer of the oral cavity on the right side. The tumor is slightly hypointense to the adjacent tissue (arrow). The ROI was placed inside the tumor on every slide (whole lesion measurement). **b** The calculated T1 histogram of the tumor. The resulting parameters were mean 5.5×10^{-4}, min 3.0×10^{-4}, max 8.3×10^{-4}, p10 4.3×10^{-4}, p25 4.9×10^{-4}, p75 6.2×10^{-4}, p90 6.6×10^{-4}, median 5.4×10^{-4}, mode 5.2×10^{-4}, SD 9.3×10^{-5}, skewness 0.16, kurtosis 2.9, and entropy 4.19. **c** The T2-weighted image. The tumor is hyperintense (arrow). **d** The estimated T2 histogram of the tumor. The calculated parameters are as follows: mean 4.9×10^{-4}, min 1.3×10^{-4}, max 9.3×10^{-4}, p10 3.5×10^{-4}, p25 4.2×10^{-4}, p75 5.5×10^{-4}, p90 6.2×10^{-4}, median 4.9×10^{-4}, mode 4.4×10^{-4}, SD 1.0×10^{-4}, skewness 0.11, kurtosis 3.1, and entropy 3.76.

Denmark; clone DO-7, dilution 1:100), HIF-1α (Biocare Medical, 60 Berry Dr. Pacheco, CA 94553; clone EP1215Y, dilution 1:100), and human papilloma virus (p16 expression, Cintec Histology, Roche, Germany) according to previous descriptions [22–24].

Furthermore, the stained specimens were digitalized (Pannoramic microscope scanner, Pannoramic SCAN, 3DHISTECH Ltd., Budapest, Hungary) and three captures with a magnification of × 200 were extracted of each sample. Histopathological features were estimated using the ImageJ software 1.48v (National Institutes of Health Image program) [8, 9, 12]. Tumor proliferation index Ki67 was estimated as a ratio: (number of stained nuclei divided by number of all nuclei) × 100 %. For the analysis, the area with the highest number of positive tumor nuclei was selected [25]. Tumor cell count was estimated as a number of all nuclei [25]. The analyzed tumors were divided into p16 positive and p16 negative based on p16 expression [19]. Expression of EGFR, VEGF, HIF-1α, and p53 (Fig. 2a, e, c, d) was estimated as a sum of stained areas (μm^2).

Statistical Analysis

The SPSS package (IBM SPSS Statistics for Windows, version 22.0, Armonk, NY: IBM corporation) was used for statistical analysis. Associations between investigated parameters were analyzed using Spearman's correlation

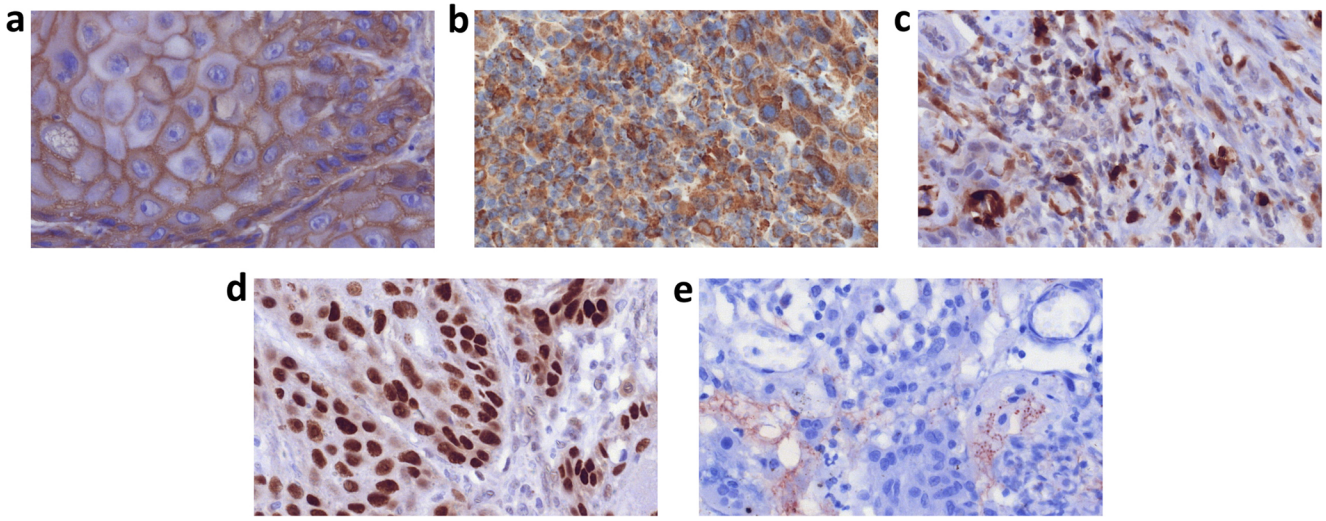

Fig. 2. Histopathological findings. **a** The EGFR-stained specimen of the patient. The stained area measures 29.014 μm^2. **b** The Her2-stained specimen of the patient. The stained area measures 59.053 μm^2. **c** The HIF-1α-stained specimen. The stained area measures 21.980 μm^2. **d** The p53-stained specimen. The stained area measures 32.778 μm^2. **e** The VEGF-stained specimen. The stained area measures 21.980 μm^2. The tumor was p16 negative (not shown). Ki67 index was 74 % (not shown). Cell count was 177 cells.

coefficient (p). Furthermore, Mann-Whitney test was used to compare the imaging parameters between p16+ and p16− groups. P values < 0.05 were taken to indicate statistical significance.

Data availability

A table about the relevant anonymous data can be provided by the authors.

Results

There were no significant differences of the analyzed parameters between p16-positive and p16-negative tumors. Correlation analysis identified several associations between the investigated parameters (Fig. 3a). In the overall sample, an inverse correlation between entropy derived from T1w images and p53 expression ($p = -0.458$, $P = 0.01$) was found. Furthermore, p10 derived from T1w images correlated with VEGF expression ($p = 0.371$, $P = 0.04$). No parameters derived from T2w images were associated with the investigated histopathological features.

In the p16-positive tumors, VEGF expression correlated as statistically significant with several parameters derived from T1w images (Fig. 3b), namely, mean ($p = 0.481$, $P = 0.032$), p10 ($p = 0.489$, $P = 0.029$), p25 ($p = 0.475$, $P = 0.034$), median ($p = 0.468$, $P = 0.037$), and mode ($p = 0.492$, $P = 0.028$). Furthermore, entropy derived from T2w images was also associated with VEGF expression ($p = -0.473$, $P = 0.035$). Additionally, several parameters derived from T2w images were associated with p53 expression, namely, mean ($p = 0.569$, $P = 0.007$), p25 ($p = 0.508$, $P = 0.019$), p75 ($p = 0.479$, $P = 0.028$), median ($p = 0.555$, $P = 0.009$), and mode ($p = 0.468$, $P = 0.033$). Also, several T2w parameters correlated moderately with Ki67 index, namely, mean ($p = 0.492$, $P = 0.023$), p75 ($p = 0.501$, $P = 0.021$), p90 ($p = 0.486$. $P = 0.025$), median ($p = 0.481$, $P = 0.027$), and mode ($p = 0.505$, $P = 0.02$). Finally, kurtosis derived from T2w images correlated as statistically significant with cell count ($p = 0.534$, $P = 0.013$). Regarding T1w parameters, only entropy was significantly associated with p53 expression ($p = -0.648$, $P = 0.001$).

For p16-negative carcinomas, fewer statistically significant correlations could be identified (Fig. 3c). So, T2w parameters correlated with p53 expression, namely, max ($p = 0.736$, $P = 0.015$), p90 ($p = 0.687$ $P = 0.028$), and standard deviation ($p = 0.760$, $P = 0.011$). In addition, p10 ($p = -0.709$, $P = 0.022$) and p25 ($p = -0.733$, $P = 0.016$) were associated with HIF-1α expression.

There were no statistically significant correlations between parameters derived from T1w images and histopathological findings in this tumor subgroup.

Discussion

To the best of our knowledge, this is the first study that identified associations between histogram parameters derived from conventional MR imaging and histopathological features in HNSCC. Furthermore, as shown, these relationships depend on tumor p16 status.

Some previous reports indicated that functional MRI modalities were able to reflect tumor microstructure and to predict tumor behavior [2–10]. For example, it has been shown that ADC values correlated moderately to strongly with cellularity in different tumor entities [5]. Also in HNSCC,

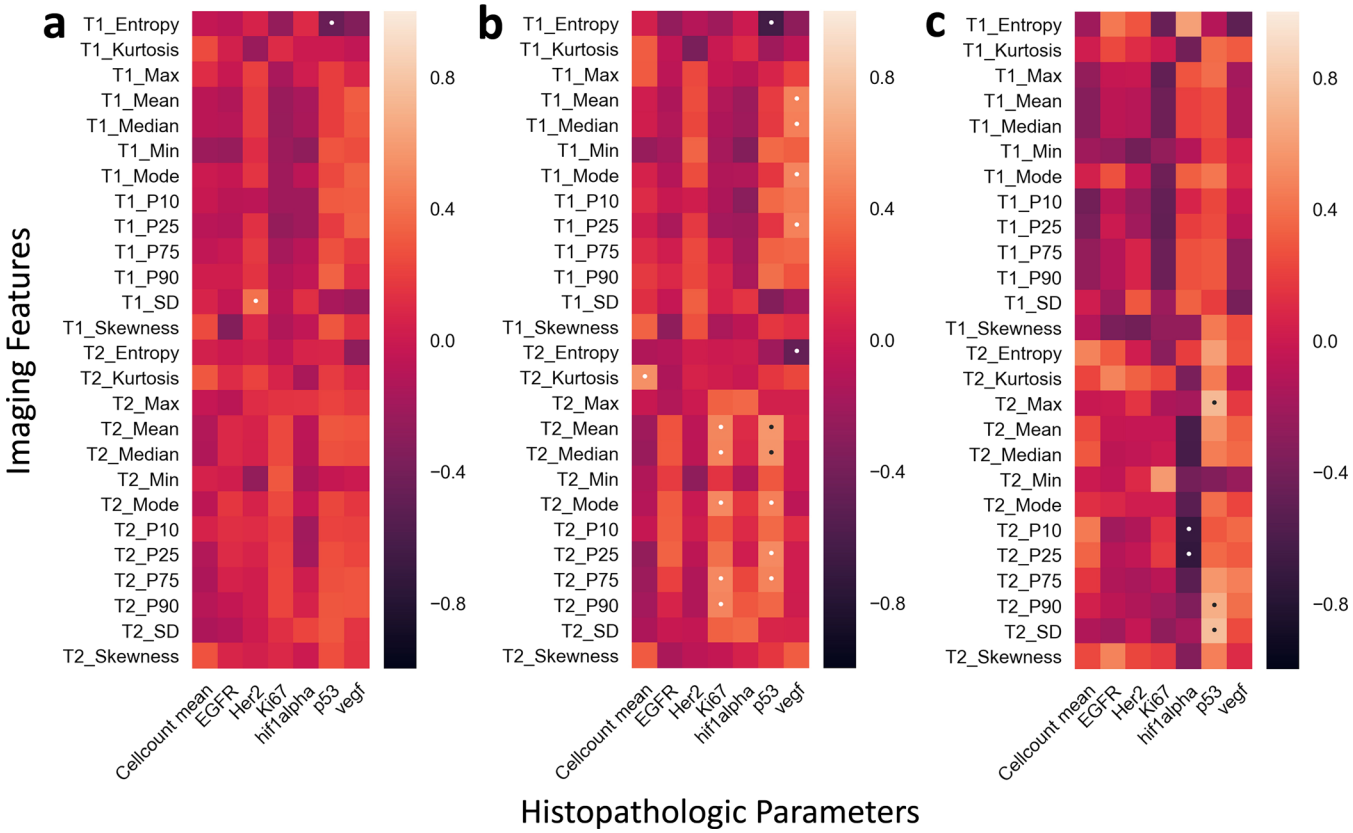

Fig. 3. Correlation analysis of the investigated parameters. **a** Correlation heat map in the overall sample. **b** Correlations between the imaging and histopathological features in p16+ tumors. **c** Correlations between the imaging and histopathological features in p16 tumors.

correlations between imaging and histopathology were reported. So, ADC parameters correlated with Ki67 expression and nucleic areas [9]. Furthermore, Ktrans derived from DCE-MRI correlated inversely with Ki67 expression, whereas Ve tended to correlate with cell count [8].

However, not only functional MRI modalities, such as DWI and/or DCE-MRI, can reflect tumor microstructure. Some preliminary studies showed that also the signal intensity derived from conventional T1w and T2w images might be linked to cellularity, when obtained images are evaluated using histogram or texture analysis [15, 16, 26]. For example, in cerebral lymphoma, the maximum signal intensity derived from FLAIR sequence correlated moderately with cellularity [15]. Moreover, parameters retrieved from post-contrast T1w images also correlated with cellularity [15]. Similar results were reported for glioblastoma [26]. These results indicate that every sequence might reflect different aspects of tumor histopathology. Presumably, these novel findings can be transferred to other tumor entities. In fact, texture analysis parameters of pre-contrast T1w and T2w images correlated with cellularity, Ki67 index, and p53 expression in thyroid cancer [16]. Similarly, in breast cancer, texture analysis parameters derived from pre-contrast T1w images were associated with Ki67 index [27].

In the present study, no significant association between cellularity and Ki67 index could be identified in the overall patient sample. However, we found that associations between imaging parameters and histopathology were different dependent on p16 status. For instance, in p16-positive tumors, several imaging parameters were associated with cell count and Ki67 index. Interestingly, the observed correlation coefficients are good compared with the previously reported correlations between ADC and Ki67 [9, 25].

Furthermore, we hypothesized that imaging parameters might be associated also with other histopathological features in HNSCC. In the present study, we elucidated further tumor features, namely hypoxic-tumor areas (HIF-1α) and tumor neoangiogenesis (VEGF), as well as tumor-promoting proteins (EGFR, p53, Her2). In fact, we also could identify that in p16-positive carcinomas, parameters retrieved from T1w images might be linked with VEGF expression indicating that T1w parameters might also be related to tumor vascularity.

Furthermore, several parameters derived from T2w images were associated with p53 expression in p16-positive carcinomas. This finding is in agreement with previous results reported by Dang et al., who performed a texture analysis of conventional sequences and identified an

accuracy of 81.3 % for correct prediction of the p53 status [28]. Moreover, several texture features, derived from T1w and T2w images, showed correlations with p53 expression in thyroid cancer [16].

As mentioned above, for p16-negative tumors, fewer statistically significant correlations between imaging parameters and histopathological findings could be identified. These differences might be caused by several reasons. It is known that p16-positive cancers are more often non-keratinized and their Ki67 expression is higher [29]. Moreover, expression profiles of p16-positive and p16-negative cancers might differ significantly emphasizing their different tumor behavior [24, 30]. So, it was shown that expression of epidermal growth factor receptor kinase substrate 8 or Eps8 was significantly lower in p16-positive than that in p16-negative tumors [30].

The observed associations between imaging and histopathology in the present study are clinically relevant. So, p16 expression is one of the most important prognostic factors in HNSCC with a more favorable outcome for p16-positive cancers [19]. EGFR regulates many cellular pathways like cell proliferation, apoptosis, and cellular differentiation [31, 32]. According to the literature, EGFR expression is a good prognostic parameter in HNSCC [31, 32]. Another factor namely p53 promotes cell cycle arrest, senescence, or apoptosis [33]. Furthermore, VEGF plays also a significant role in HNSCC. Previous reports suggested that overexpression of VEGF is a poor indicator for patients with head and neck cancer [34]. Finally, HIF-1α can also predict prognosis in HNSCC. Overexpression of HIF-1α is associated with poor survival in HNSCC [35]. This histopathological parameter characterizes cellular responses to hypoxic stress and is related to the neoangiogenesis [35]. As shown, some imaging parameters may be used as a surrogate marker for tumor cellularity, proliferation potential, and expression of p53 and VEGF.

We could not identify statistically significant differences between p16-positive and p16-negative carcinomas. According de Perrot et al., ADC histogram analysis parameters can be used to differentiate between p16-positive and p16-negative tumors [29]. Presumably, histogram analysis derived from conventional sequences might not be able to reflect such differences of microstructure between these groups.

The present study has several limitations. Firstly, our patient sample is relatively small. Secondly, we performed a whole-tumor measurement to estimate the imaging parameters. However, histopathological features were analyzed on a small part of the tumor (tumor biopsy). This fact might limit our results. Thirdly, our imaging analysis was performed by an in-house programmed Matlab tool, which might hinder the repeatability by other researchers. However, we used validated formulas for calculation of skewness, kurtosis, and entropy and, therefore, similar programs can be easily established. Clearly, further studies with more patients are needed to confirm our preliminary results.

Conclusion

The present study revealed multiple associations between histogram parameters derived from T1w and T2w images and clinically relevant histopathological features in HNSCC. Therefore, imaging parameters can be also used as surrogate markers for tumor cellularity, proliferation, and vascularization in HNSCC. Furthermore, the identified correlations differed significantly between p16-positive and p16-negative cancers that may reflect different tumor behaviors of these entities.

Authors' Contribution. Conception and design: H.J. Meyer, A. Surov
Development of methodology: H.J. Meyer, L. Leifels, A.K. Höhn, A. Surov
Acquisition of data (provided animals, acquired and managed patients, provided facilities, *etc.*): H.J. Meyer, L. Leifels, G. Hamerla, A.K. Höhn, A. Surov
Analysis and interpretation of data (*e.g.*, statistical analysis, biostatistics, computational analysis): H.J. Meyer, L. Leifels, G. Hamerla, A.K. Höhn
Writing, review, and/or revision of the manuscript: H.J. Meyer, A. Surov
Administrative, technical, or material support (*i.e.*, reporting or organizing data, constructing databases): G. Hamerla, A.K. Höhn
Study supervision: A. Surov

Compliance with Ethical Standards

Conflict of Interest

The authors declare that they have no conflict of interest.

Ethics Approval and Consent to Participate

This study adhered to the principles of the Declaration of Helsinki II and was approved by the Institutional Review Board of the University of Leipzig (ethics committee of the University of Leipzig, study codes 180-2007, 201-10-12072010, and 341-15-05102015). Written informed consent was obtained from all the study participants.

References

1. Braakhuis BJ, Leemans CR, Visser O (2014) Incidence and survival trends of head and neck squamous cell carcinoma in the Netherlands between 1989 and 2011. Oral Oncol 50:670–675
2. Szyszko TA, Cook GJR (2018) PET/CT and PET/MRI in head and neck malignancy. Clin Radiol 73:60–69
3. Padhani AR, Liu G, Koh DM et al (2009) Diffusion-weighted magnetic resonance imaging as a cancer biomarker: consensus and recommendations. Neoplasia 11:102–125
4. O'Connor JP, Aboagye EO, Adams JE et al (2017) Imaging biomarker roadmap for cancer studies. Nat Rev Clin Oncol 14:169–186
5. Surov A, Meyer HJ, Wienke A (2017) Correlation between apparent diffusion coefficient (ADC) and cellularity is different in several tumors: a meta-analysis. Oncotarget 8:59492–59499
6. Surov A, Meyer HJ, Wienke A (2017) Associations between apparent diffusion coefficient (ADC) and KI 67 in different tumors: a meta-analysis. Part 1: ADC_{mean}. Oncotarget 8:75434–75444
7. Little RA, Barjat H, Hare JI, Jenner M, Watson Y, Cheung S, Holliday K, Zhang W, O'Connor JPB, Barry ST, Puri S, Parker GJM, Waterton JC (2018) Evaluation of dynamic contrast-enhanced MRI biomarkers for stratified cancer medicine: how do permeability and perfusion vary between human tumours? Magn Reson Imaging 46:98–105
8. Surov A, Meyer HJ, Gawlitza M, Höhn AK, Boehm A, Kahn T, Stumpp P (2017) Correlations between DCE MRI and histopathological parameters in head and neck squamous cell carcinoma. Transl Oncol 10:17–21

9. Surov A, Stumpp P, Meyer HJ et al (2016) Simultaneous (18)F-FDG-PET/MRI: associations between diffusion, glucose metabolism and histopathological parameters in patients with head and neck squamous cell carcinoma. Oral Oncol 58:14–20
10. Driessen JP, Caldas-Magalhaes J, Janssen LM, Pameijer FA, Kooij N, Terhaard CHJ, Grolman W, Philippens MEP (2014) Diffusion-weighted MR imaging in laryngeal and hypopharyngeal carcinoma: association between apparent diffusion coefficient and histologic findings. Radiology 272:456–463
11. Just N (2014) Improving tumour heterogeneity MRI assessment with histograms. Br J Cancer 111:2205–2213
12. Schob S, Meyer HJ, Pazaitis N, Schramm D, Bremicker K, Exner M, Höhn AK, Garnov N, Surov A (2017) ADC histogram analysis of cervical cancer aids detecting lymphatic metastases—a preliminary study. Mol Imaging Biol 19:953–962
13. Liu S, Zhang Y, Chen L et al (2017) Whole-lesion apparent diffusion coefficient histogram analysis: significance in T and N staging of gastric cancers. BMC Cancer 17:665
14. Meyer HJ, Leifels L, Schob S et al (2018) Histogram analysis parameters identify multiple associations between DWI and DCE MRI in head and neck squamous cell carcinoma. Magn Reson Imaging 45:72–77
15. Meyer HJ, Schob S, Münch B, Frydrychowicz C, Garnov N, Quäschling U, Hoffmann KT, Surov A (2018) Histogram analysis of T1-weighted, T2-weighted, and postcontrast T1-weighted images in primary CNS lymphoma: correlations with histopathological findings—a preliminary study. Mol Imaging Biol 20:318–323
16. Meyer HJ, Schob S, Höhn AK, Surov A (2017) MRI texture analysis reflects histopathology parameters in thyroid cancer—a first preliminary study. Transl Oncol 10:911–916
17. Wu X, Sikiö M, Pertovaara H, Järvenpää R, Eskola H, Dastidar P, Kellokumpu-Lehtinen PL (2016) Differentiation of diffuse large B-cell lymphoma from follicular lymphoma using texture analysis on conventional mr images at 3.0 tesla. Acad Radiol 23:696–703
18. Ko ES, Kim JH, Lim Y, Han BK, Cho EY, Nam SJ (2016) Assessment of invasive breast cancer heterogeneity using whole-tumor magnetic resonance imaging texture analysis: correlations with detailed pathological findings. Medicine (Baltimore) 95:e2453
19. Fischer CA, Kampmann M, Zlobec I, Green E, Tornillo L, Lugli A, Wolfensberger M, Terracciano LM (2010) P16 expression in oropharyngeal cancer: its impact on staging and prognosis compared with the conventional clinical staging parameters. Ann Oncol 21:1961–1966
20. Swartz JE, Pothen AJ, Stegeman I, Willems SM, Grolman W (2015) Clinical implications of hypoxia biomarker expression in head and neck squamous cell carcinoma: a systematic review. Cancer Med 4:1101–1116
21. Solomon MC, Vidyasagar MS, Fernandes D, Guddattu V, Mathew M, Shergill AK, Carnelio S, Chandrashekar C (2016) The prognostic implication of the expression of EGFR, p53, cyclin D1, Bcl-2 and p16 in primary locally advanced oral squamous cell carcinoma cases: a tissue microarray study. Med Oncol 33:138
22. Rasmussen GB, Vogelius IR, Rasmussen JH, Schumaker L, Ioffe O, Cullen K, Fischer BM, Therkildsen MH, Specht L, Bentzen SM (2015) Immunohistochemical biomarkers and FDG uptake on PET/CT in head and neck squamous cell carcinoma. Acta Oncol 54:1408–1415
23. Grönroos TJ, Lehtiö K, Söderström KO, Kronqvist P, Laine J, Eskola O, Viljanen T, Grénman R, Solin O, Minn H (2014) Hypoxia, blood flow and metabolism in squamous-cell carcinoma of the head and neck: correlations between multiple immunohistochemical parameters and PET. BMC Cancer 14:876
24. Troy JD, Weissfeld JL, Youk AO, Thomas S, Wang L, Grandis JR (2013) Expression of EGFR, VEGF, and NOTCH1 suggest differences in tumor angiogenesis in HPV-positive and HPV-negative head and neck squamous cell carcinoma. Head Neck Pathol 7:344–355
25. Surov A, Meyer HJ, Winter K, Richter C, Hoehn AK (2018) Histogram analysis parameters of apparent diffusion coefficient reflect tumor cellularity and proliferation activity in head and neck squamous cell carcinoma. Oncotarget 9:23599–23607
26. Chang PD, Malone HR, Bowden SG et al (2017) A multiparametric model for mapping cellularity in glioblastoma using radiographically localized biopsies. AJNR Am J Neuroradiol 38:890–898
27. Holli-Helenius K, Salminen A, Rinta-Kiikka I, Koskivuo I, Brück N, Boström P, Parkkola R (2017) MRI texture analysis in differentiating luminal A and luminal B breast cancer molecular subtypes—a feasibility study. BMC Med Imaging 17:69
28. Dang M, Lysack JT, Wu T, Matthews TW, Chandarana SP, Brockton NT, Bose P, Bansal G, Cheng H, Mitchell JR, Dort JC (2015) MRI texture analysis predicts p53 status in head and neck squamous cell carcinoma. AJNR Am J Neuroradiol 36:166–170
29. de Perrot T, Lenoir V, Domingo Ayllón M, Dulguerov N, Pusztaszeri M, Becker M (2017) Apparent diffusion coefficient histograms of human papillomavirus-positive and human papillomavirus-negative head and neck squamous cell carcinoma: assessment of tumor heterogeneity and comparison with histopathology. AJNR Am J Neuroradiol 38:2153–2160
30. Nasri E, Wiesen LB, Knapik JA, Fredenburg KM (2018) Eps8 expression is significantly lower in p16+ head and neck squamous cell carcinomas (HNSCCs) compared with p16- HNSCCs. Hum Pathol 72:45–51
31. Bossi P, Resteghini C, Paielli N, Licitra L, Pilotti S, Perrone F (2016) Prognostic and predictive value of EGFR in head and neck squamous cell carcinoma. Oncotarget 7(45):74362–74379
32. Ma X, Huang J, Wu X, Li X, Zhang J, Xue L, Li P, Liu L (2014) Epidermal growth factor receptor could play a prognostic role to predict the outcome of nasopharyngeal carcinoma: a meta-analysis. Cancer Biomark 14:267–277
33. Tandon S, Tudur-Smith C, Riley RD, Boyd MT, Jones TM (2010) A systematic review of p53 as a prognostic factor of survival in squamous cell carcinoma of the four main anatomical subsites of the head and neck. Cancer Epidemiol Biomark Prev 19:574–587
34. Zang J, Li C, Zhao LN, Shi M, Zhou YC, Wang JH, Li X (2013) Prognostic value of vascular endothelial growth factor in patients with head and neck cancer: a meta-analysis. Head Neck 35:1507–1514
35. Gong L, Zhang W, Zhou J, Lu J, Xiong H, Shi X, Chen J (2013) Prognostic value of HIFs expression in head and neck cancer: a systematic review. PLoS One 8:e75094